Numerical studies of two-dimensional hydroelastic periodic and generalised solitary waves

Tao Gao[1, a)] and Jean-Marc Vanden-Broeck[1, b)]

Department of Mathematics, University College London, Gower Street, London WC1E 6BT, UK

(Dated: 7 April 2014)

Hydroelastic waves propagating at a constant velocity at the surface of a fluid are considered. The flow is assumed to be two-dimensional and potential. Gravity is included in the dynamic boundary condition. The fluid is bounded above by an elastic sheet which is described by the Plotnikov-Toland model. Fully nonlinear solutions are computed by a series truncation method. The findings generalised previous results where the sheet was described by a simplified model known as the Kirchhoff-Love model. Periodic and generalised solitary waves are computed. The results strongly suggest that there are no true solitary waves (i.e. solitary waves characterised by a flat free surface in the far field). Detailed comparisons with results obatained with the Kirchhoff-Love model and for the related problem of gravity capillary waves are also presented.

PACS numbers: 47.11.Kb, 47.35.Fg, 47.85.Dh

[a)] tao.gao.10@ucl.ac.uk

[b)] j.vanden-broeck@ucl.ac.uk

I. INTRODUCTION

The problems of hydroelasticity have many applications in biology, medicine and industry. They are also relevant to polar engineering where ice sheets are modelled by elastic sheets. The reader is refered to[1] for a review and references.

Early work on the subject was based on the Kirchhoff-Love elastic model (refered to as the KL model). It was for example used in[2] and[3] to calculate large amplitude periodic waves. Two-dimensional solitary waves were later studied in[4] and three-dimensional configurations were investigated in[5]. The dynamics and the stability of hydroelastic solitary waves were considered in[6] and dark solitons were calculated in[7]. In most of these works, the boundary integral equation method, first introduced for the gravity-capillary problem in[8], was adapted for solving the fully nonlinear hydroelastic problem. In[9] a different numerical method (based on a truncated Laurent series) was used to compute periodic and generalised solitary waves.

More recently a new nonlinear model for elastic sheet was introduced by Plotnikov and Toland[10]. It uses the special Cosserat theory of hyperelatic shells with Kirchhoff's hypotheses to express the pressure P exerted by the elastic sheet on the water as

$$P = D(\kappa_{ss} + \frac{1}{2}\kappa^3). \tag{1}$$

Here D is the flexural rigidity, κ is the curvature of the free surface and s is the arclength. Solitary waves were studied by using this model in[11,12]. Time-dependent solutions and periodic waves were also computed in these papers. The Plotnikov and Toland has the advantage over the KL model that it conserves the elastic potential energy.

In this paper, we use the Plotnikov and Toland's model and the series truncation method to study periodic and generalised solitary waves. The problem is formulated in Section II and the numerical scheme is described in Section III. Numerical results are presented in Section IV. They strongly suggest that there are no true solitary waves (i.e. the amplitude of the ripples of the generalised solitary waves does not vanish for any choice of the parameters). A comparison with the results given by the KL model is presented in Section V. The corresponding properties of gravity-capillary waves are also discussed in Section V. Concluding remarks are given in Section VI.

II. FORMULATION

We consider a two-dimensional irrotational flow of an inviscid and incompressible fluid of constant depth h, covered by an elastic sheet. The free-surface (i.e. the upper surface of the fluid) is deformed by a train of waves travelling at a constant velocity c. The configuration is illustrated in Figure 1.

We introduce a two-dimensional cartesian system with the y-axis pointing upwards. We denote by $y = \eta(x)$ the equation of the (unknown) free-surface. The level of the bottom is chosen to be $y = -h$. The acceleration of gravity g acts in the negative y-direction. A frame of reference moving with the waves is chosen so that the flow is steady. We introduce the potential function ϕ and the streamfunction ψ. We choose $\psi = 0$ on the free-surface and $\phi = 0$ at the crest where $x = 0$. We denote by $-Q$ the value of the streamfunction ψ on the bottom.

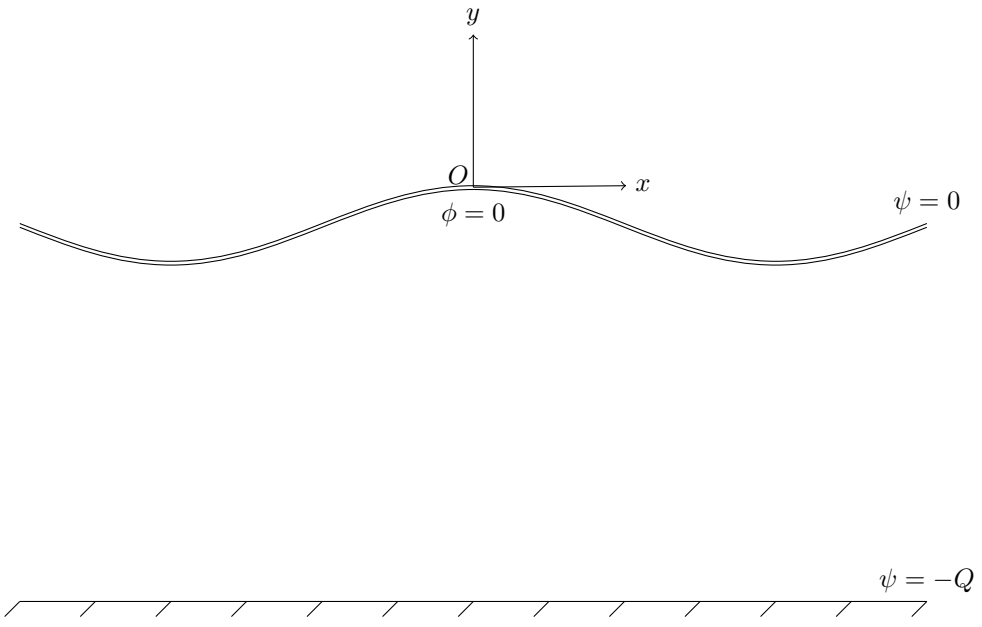

FIG. 1. The mathematical configuration of the problem.

The governing equations are as follows

$$\nabla^2\phi = 0, \qquad -h < y < \eta(x), \tag{2}$$

$$\phi_y = \phi_x\eta_x, \qquad \text{on } y = \eta(x), \tag{3}$$

$$\frac{1}{2}(\phi_x^2 + \phi_y^2) + gy + \frac{P}{\rho} = B, \qquad \text{on } y = \eta(x), \tag{4}$$

$$\phi_y = 0, \qquad \text{on } y = -h, \tag{5}$$

where P is the pressure exerted by the sheet on the fluid. We shall use the model proposed by Plotnikov and Toland[10] where P is defined in (1). In Section V, we will also use the KL model in which (1) is replaced by

$$P = D\kappa_{xx}. \tag{6}$$

Equation (3) and (5) are the kinematic boundary conditions on the free-surface and on the bottom respectively. Equatioin (4) is the Bernoulli equation on the free-surface or, in other words, the dynamic boundary condition and B is the Bernoulli constant.

We use the potential function ϕ and the streamfunction ψ as the independent variables. We then introduce the complex velocity $w = u - iv$ and write

$$u - iv = ce^{\tau - i\theta} \tag{7}$$

The function $\tau(\phi,\psi) - i\theta(\phi,\psi)$ is an analytic function of the complex potential $\phi + i\psi$. The definition 7 implies

$$x_\phi + iy_\phi = \frac{1}{u - iv} = \frac{1}{c}e^{-\tau + i\theta} \tag{8}$$

whose real part and imaginary parts can be used to find x and y by integrating with respect to ϕ.

Then (4) becomes

$$\frac{c^2}{2}e^{2\tau(\phi,0)} + \frac{g}{c}\int_0^\phi e^{-\tau(\varphi,0)}\sin[\theta(\varphi,0)]d\varphi + \frac{D}{\rho}(\partial_{ss}\kappa + \frac{1}{2}\kappa^3) = B. \tag{9}$$

By using the chain rule, we have

$$\partial_s\kappa = \partial_s\phi\partial_\phi\kappa + \partial_s\psi\partial_\psi\kappa = ce^\tau\kappa_\phi. \tag{10}$$

where we have used the property that ψ is constant on the free-surface. Since $\kappa = ce^\tau\theta_\phi$ and we obtain after some algebra

$$\kappa_{ss} + \frac{1}{2}\kappa^3 = c^3e^{3\tau}(\theta_{\phi\phi\phi} + 3\tau_\phi\theta_{\phi\phi} + \tau_{\phi\phi}\theta_\phi + 2\tau_\phi^2\theta_\phi + \frac{\theta_\phi^3}{2}). \tag{11}$$

We note that a formulation similar to that described in this section was used before in[9] for the KL model.

III. NUMERICAL SCHEME

The flow domain in the complex potential plane is the strip $-Q < \psi < 0$. The kinematic boundary condition on the bottom can be satisfied by using the method of images. Then we have $\psi = -2Q$ on the image of the free-surface into the bottom. Hence the extended flow domain is the strip $-2Q < \psi < 0$. Then we perform the conformal mapping

$$t = e^{-\frac{2i\pi f}{c\lambda}}, \tag{12}$$

where $f = \phi + i\psi$ is the complex potential and λ is the wavelength. It maps the strip onto the annulus $r_0^2 < |t| < 1$, where

$$r_0 = e^{\frac{-2\pi Q}{c\lambda}}. \tag{13}$$

Since w is an analytic function of f, so is $\tau - i\theta$. Hence $\tau - i\theta$ is an analytic function of t which can be represented by the Laurent series

$$\tau - i\theta = a_0 + \sum_{n=1}^{\infty} a_n t^n + \sum_{n=1}^{\infty} b_n t^{-n}. \tag{14}$$

Since $\psi = -2Q$ is the image of the surface $\psi = 0$, we obtain

$$\tau(\phi, 0) - i\theta(\phi, 0) = \tau(\phi, -2Q) + i\theta(\phi, -2Q). \tag{15}$$

Combining (14) and (15) gives

$$b_n = a_n r_0^{2n}. \tag{16}$$

We choose c as the unit velocity and Q/c as the unit length. In the dimensionless form, (9) becomes

$$\frac{1}{2}e^{2\tau} + \frac{1}{F^2}\int_0^{\phi} e^{-\tau(\varphi)} \sin[\theta(\varphi)] d\varphi + \beta(\kappa_{ss} + \frac{1}{2}\kappa^3) = B, \tag{17}$$

where B is the dimensionless Bernoulli constant,

$$F = \frac{c}{\sqrt{gh}} \tag{18}$$

is the Froude number and

$$\beta = \frac{Dc}{\rho Q^3}. \tag{19}$$

One can easily rewrite (13) as

$$r_0 = e^{\frac{-2\pi}{l}} \tag{20}$$

where l is the dimensionless wavelength. By substituting (12) into (14) and truncating the series after $N-2$ terms, we get

$$\tau = a_0 + \sum_{n=1}^{N-2} \cos(kn\phi)(1 + r_0^{2n})a_n, \tag{21}$$

$$\theta = \sum_{n=1}^{N-2} \sin(kn\phi)(1 - r_0^{2n})a_n. \tag{22}$$

Now we introduce $N-1$ collocation points uniformly distributed in $[0, \frac{l}{2}]$,

$$\phi_I = \frac{l}{2}\frac{I-1}{N-2}, \quad I = 1, 2, ...N-1. \tag{23}$$

The dynamic boundary condition (17) is satisfied at these points, which yields $N-1$ algebraic equations. The periodicity of the wave implies

$$x = \frac{l}{2} \quad \text{when } \phi = \frac{l}{2}. \tag{24}$$

Fixing the amplitude gives the additional equation

$$|y(\frac{l}{2}) - y(0)| = A = \bar{s}l, \tag{25}$$

where $\bar{s}$ is the steepness (i.e. the difference of heights between a crest and a trough divided by the wavelength) and A is the amplitude. By fixing β, A and l, the resulting system with $N+1$ equations and $N+1$ unknowns $(a_0, a_1, ..., a_{N-2}, B, b)$ can be solved by Newton's method. The error of the numerical solution obtained by Newton's method is set to be less than 10^{-10}. Once the solution is obtained, one can get the values of x and y by integrating x_ϕ and y_ϕ respectively. This gives the profile of the wave.

A. Case of infinite depth

In the case of infinite depth, the numerical scheme remains valid except that we now use the reference length $(D/\rho c^2)^{\frac{1}{3}}$ since Q/c tends to infinity as the depth tends to infinity. Following (13), $r_0 = 0$ since h tends to infinity and so $b_n = 0$ by (16). The dynamic boundary condition (9) becomes

$$\frac{1}{2}e^{2\tau} + \gamma \int_0^\phi e^{-\tau(\varphi)} \sin[\theta(\varphi)]d\varphi + [\partial_s^2\kappa + \frac{1}{2}\kappa^3] = B, \tag{26}$$

where

$$\gamma = (Dg^3/\rho c^8)^{\frac{1}{3}}. \tag{27}$$

We note that γ is related to the phase velocity c. In Section IV A we use this parameter to test the numerical accuracy.

IV. DISCUSSION OF RESULTS

A. Numerical Accuracy

We check the convergence and accuracy of our numerical procedure in the particular case of infinite depth. When the amplitude of the waves is small, the equations of Section II can be linearised and solved analytically. The (linear) dispersion relation of the waves is then

$$c^2 = \frac{g}{k} + \frac{D}{\rho}k^3 \tag{28}$$

where $k = 2\pi/\lambda$ is the wavenumber. Using the dimensionless variables of Section III A, we can rewrite (28) as

$$\gamma = k - k^4, \tag{29}$$

where γ is defined by (27). Now we consider the quantity e defined by

$$e = |\gamma_n - \gamma_t|, \tag{30}$$

where γ_t is the theoretical value predicted by (29) and γ_n is the corresponding numerical value given by the numerical procedure of Section III. From Table I, it can be seen in the column of $s = 0.001$ and $s = 0.002$ that e converges quickly to a value that is essentially equal to zero as the number of collocation points increases. It can also be seen from the last two columns of Table I that the numerical values of γ for periodic waves of finite amplitude are different from the values of γ_t obtained from the linear dispersion relation (29) because of the nonlinearity. We compute γ_n for different values of N. Table II shows that γ_n converges quickly as N increases. In most of the computations presented in this paper we used $N = 500$.

		Error			
Wavelength	N	$s = 0.001$	$s = 0.002$	$s = 0.1$	$s = 0.2$
10	20	1.08×10^{-3}	1.08×10^{-3}	1.50×10^{-3}	1.74×10^{-2}
10	100	3.96×10^{-5}	3.95×10^{-5}	4.06×10^{-4}	1.64×10^{-2}
10	500	1.52×10^{-6}	1.41×10^{-6}	3.66×10^{-4}	1.63×10^{-2}
10	1000	3.51×10^{-7}	2.37×10^{-7}	3.65×10^{-4}	1.63×10^{-2}
10	2000	5.90×10^{-8}	5.56×10^{-8}	3.65×10^{-4}	1.63×10^{-2}

TABLE I. The values of e for periodic waves of small and finite amplitude.

		γ			
Wavelength	N	$s = 0.1$	$s = 0.15$	$s = 0.2$	$s = 0.25$
10	20	0.47396	0.47717	0.48989	0.54572
10	100	0.47287	0.47605	0.48883	0.54475
10	500	0.47283	0.47601	0.48879	0.54471
10	1000	0.47283	0.47601	0.48879	0.54471
10	2000	0.47283	0.47601	0.48879	0.54471

TABLE II. The values of γ for periodic waves of finite amplitude.

B. Periodic waves in infinite depth

A weakly nonlinear theory can be developped by expanding the solution in powers of a parameter ϵ which measures the amplitude of the wave. Vanden-Broeck and Parau[9] developped the theory up to order ϵ^2 for the KL model. Their results apply also to the Plotnikov-Toland model because the KL model and the Plotnikov-Toland model agree up to order ϵ^2. In particular, the function $\eta(x)$ of Section II is written as

$$\eta(x) = \epsilon\eta_1(x) + \epsilon^2\eta_2(x) + O(\epsilon^3), \tag{31}$$

It is found that

$$\eta_1(x) = A_1 \cos kx, \tag{32}$$

provided

$$g + \frac{D}{\rho}n^4k^4 - c_0^2nk \neq 0 \tag{33}$$

for all integer value of $n \geq 2$. Here c_0 is the value of c predicted by (28). The value of A_1 depends on the particular definition of ϵ. Vanden-Broeck and Parau[9] chose

$$\epsilon = \frac{a}{\lambda}, \tag{34}$$

where a is the first Fourier coefficient of $\eta(x)$. It then follows that $A_1 = \lambda$.

When there exists an integer $m \geq 2$ such that

$$g + \frac{D}{\rho} m^4 k^4 - c_0^2 mk = 0, \tag{35}$$

then

$$\eta(x) = A_1 \cos kx + A_m \cos mkx. \tag{36}$$

In particular when $m = 2$, it is shown in[9] that

$$A_2 = \pm \frac{1}{2} A_1, \tag{37}$$

The two profiles corresponding to (36) with $m = 2$ have a crest or a trough dimple (see the portion of Figure 2 corresponding to $m = 2$). These solutions (known as Wilton ripples) were first calculated for gravity-capillary waves (see for example[9,13] for details). The corresponding solutions for $m > 2$ become more and more tedious to calculate analytically as m increases. However they can easily be computed by using the numerical procedure of Section III. To achieve this we need to make an appropriate intial guess for $(a_0, a_1, ..., a_{N-2}, B, \gamma)$ in the Newton's iterations. The value of k can be predicted by (28) and (35) for different values of m. Then the value of γ can be easily computed by using (27). We choose $a_1 = -0.1$ and set all the remaining coefficients equal to zero. This completes the initial guess which leads to a nonlinear solution by Newton's iterations. In deep water, as explained in[9], there exist many different families of periodic waves with dimples on their free-surface. This is confirmed by the present numerical results. Some typical free-surface profiles are presented in Figure 2. These results show that more and more dimples appear on the free surface profiles as m increases.

C. Periodic waves in finite depth

The infinite depth numerical results for Figure 2 can be extended to finite depth by assuming $r_0 \neq 0$. As expected by analogy with the infinite depth results, there are again

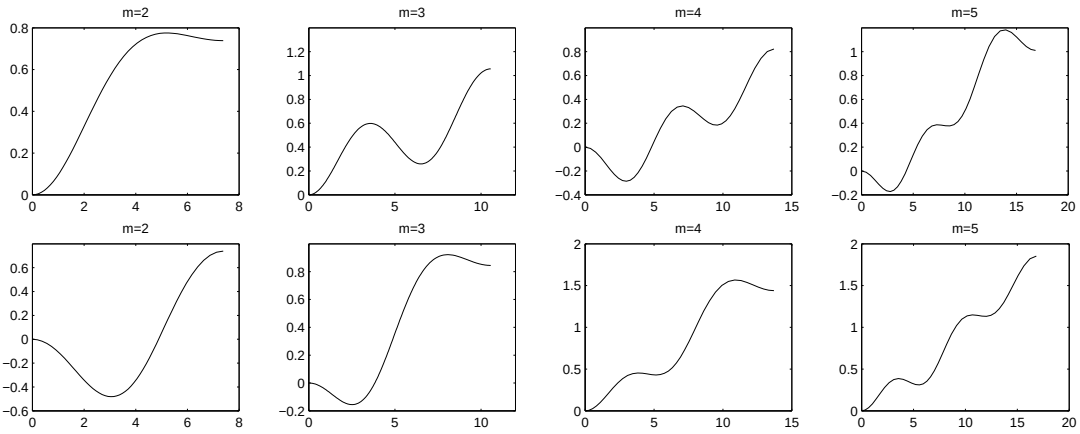

FIG. 2. Typical surface profiles for order $m = 2, 3, 4, 5$ in deep water. Only half of a wavelength of the waves is shown.

dimples on the free surface. However as the wavelength l increases (i.e. as r_0 in (20) approaches 1) these dimples tend to concentrate in the troughs of the waves (see Figure 3). These results suggest that as $l \to \infty$, the waves approach solitary waves characterised by a train of ripples of constant amplitude in the far field. Such waves are called generalised solitary waves to contrast then to true solitary waves which are characterised by a flat free surface in the far field.

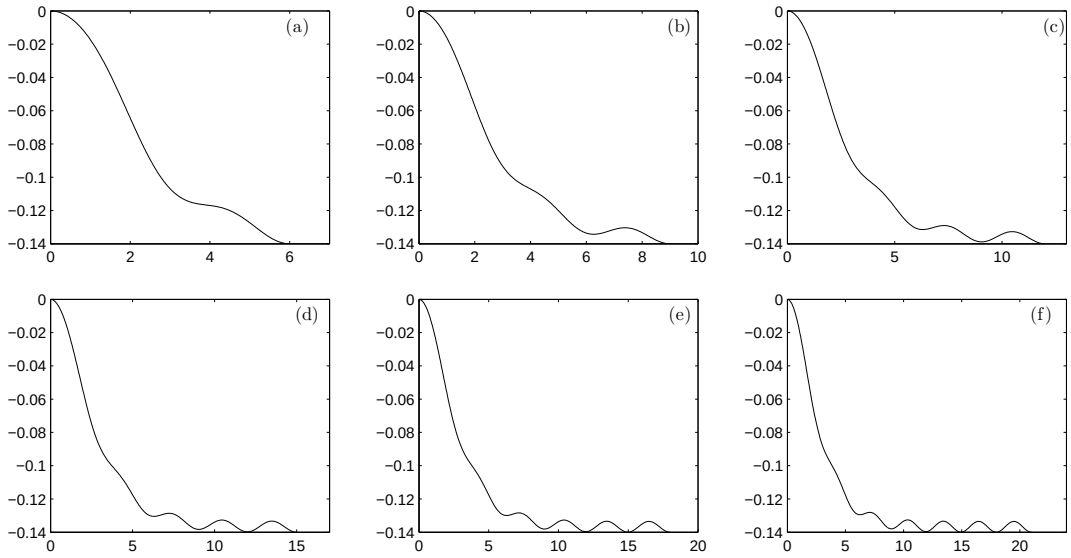

FIG. 3. Surface profiles in the case of finite depth for $\beta = 0.07$ and $A = 0.14$: the half wavelength $l/2$ equals (a) 6, (b) 9, (c) 12, (d) 15, (e) 18, (f) 21. Only half of a wavelength of the waves is shown.

D. Generalised Solitary Waves

In order to confirm the existence of generalised solitary waves, we repeated the computations of Figure 3 for larger values of l and various values of β and A. We present in Figure

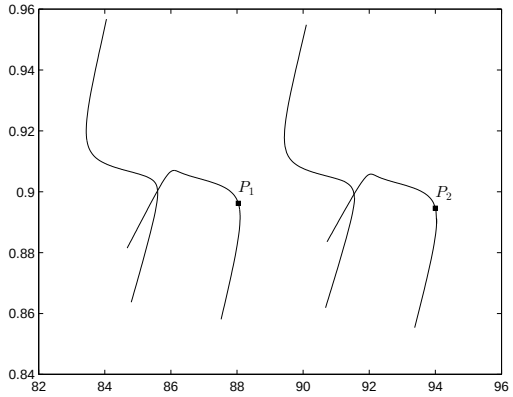

FIG. 4. The graphs of $1/F^2$ versus the wavelength l for $\beta = 0.07$ and $A = 0.14$.

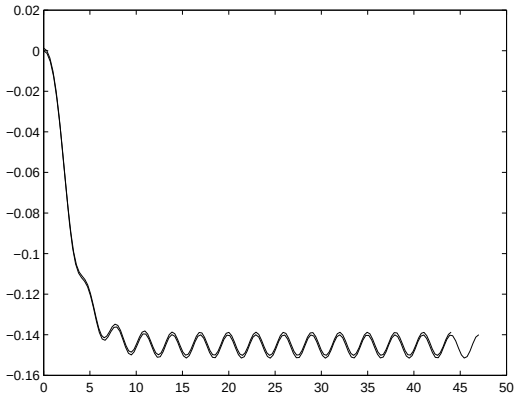

FIG. 5. The two profiles corresponding to P_1 and P_2 in Figure 4. The vertical scale has been exaggerated to show the difference of these two profiles.

4 values of $1/F^2$ versus l for $\beta = 0.07$ and $A = 0.14$. These results illustrate that there are an infinite number of branches of solutions which approach parallel curves as $l \to \infty$. Two such branches are shown in Figure 4. To explain this property we present in Figure 5 two profiles corresponding to the points P_1 and P_2 in Figure 4. We see that these two profiles are very close to each other except that the one corresponding to P_2 has one more "wavelength

of ripples" in the far field. This implies that the distance between the two parallel curves of Figure 4 is approximately equal to twice the wavelength of the ripples in the tail of the waves (this becomes exact as $l \to \infty$). Generalised solitary waves are then obtained by jumping from one curve (such as those in Figure 4) to the next as we take the limit $l \to \infty$. After each jump, two more wavelengths of the ripples appear (one on the right and one on the left). In the limit $l \to \infty$, we obtain a generalised solitary wave characterised by infinite train of ripples in the far field. For each value of β, these generalised solitary waves form a two-parameter family of solutions.

We consider a particular family for $89 < l < 95$ which is shown in Figure 6 (since l is large, it provides an approximation of generalised solitary waves). Two sub-branches of solutions are discovered. The intersection illustrates the fact that it is possible to have two different generalised solitary waves with the same wavelength and the same Froude number. Some typical free surface profiles for the left sub-branch and the right sub-branch are shown in Figure 7 and Figure 8 respectively. From Figure 7, it can be seen that the waves start

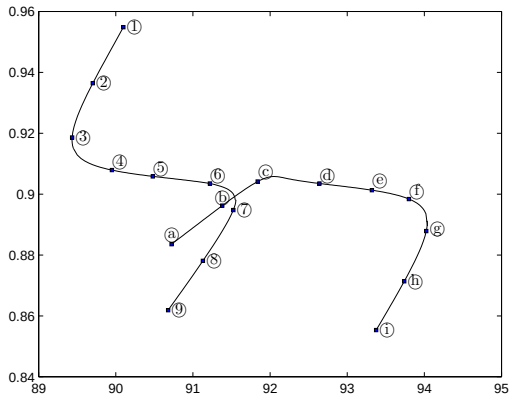

FIG. 6. The graph of $1/F^2$ versus the wavelength for a particular family when $\beta = 0.07$ and $A = 0.14$.

with large ripples and then evolve to generalised solitary waves with small ripples which enlarge again in the later stage. From Figure 8, one can again observe first very large ripples which become smaller and then larger again. The main difference is that the right-end point of the solutions from the left branch is a trough whereas the one from the right branch is a crest.

Alternatively we may impose a different condition instead of (25). For example, we can

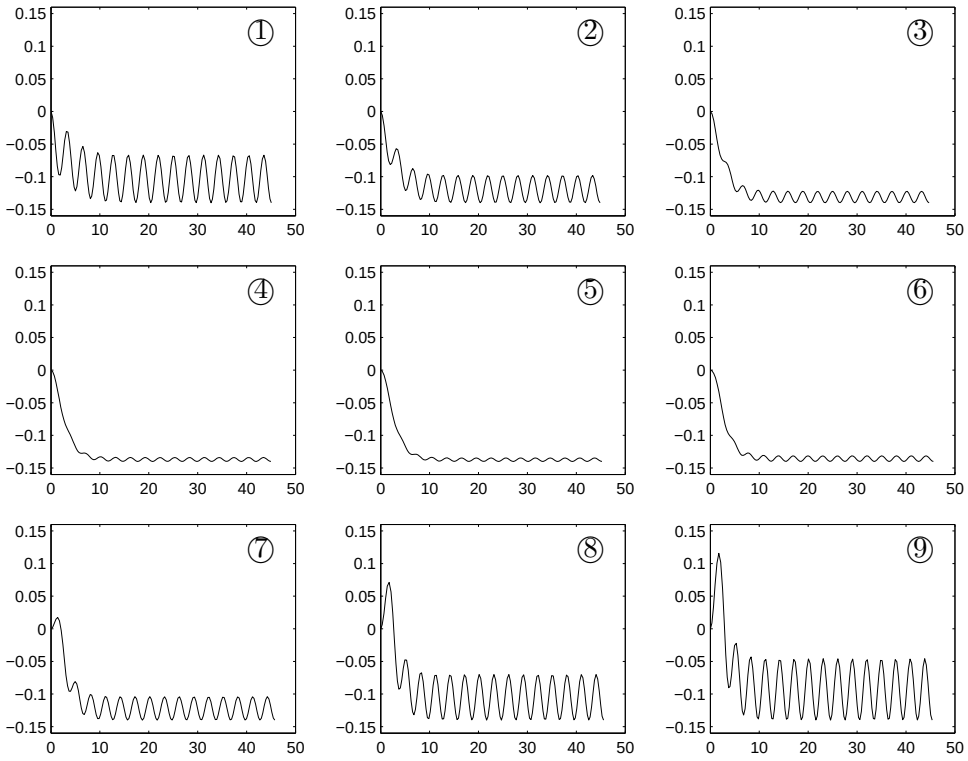

FIG. 7. Typical surface profiles from the left branch. Only half of a wavelength is shown.

fix the value u_0 of the velocity at $x = 0$. This condition was already considered in[14] for the gravity-capillary problem. Accordingly, we replace equation (25) by

$$\tau(0, 0) = \ln u_0. \tag{38}$$

We present values of $1/F^2$ versus l for $u_0 = 0.97$ and $\beta = 0.07$ in Figure 9. The value of $1/F^2$ changes little as the wavelength varies since the vertical scaling is small. The function is monotonically decreasing in each family and will eventually converges to a limit as the wavelength tends to infinity. Unlike what we have seen in Figure (6), we have only found a single branch rather than two. Examining profiles on two consecutive families in Figure 9, we found that one corresponds to the waves whose right-end point is a crest while the other one has a trough as its right-end point. Similar results are found in the case of gravity-capillary waves. (see Section V).

The ripples in the tail of generalised solitary waves are of questionable physical validity because they occur on both sides and therefore do not satisfy the radiation condition. Therefore an important question is whether or not the parameters can be chosen so that the amplitude of the ripples vanish. To investigate this question we choose the absolute value of

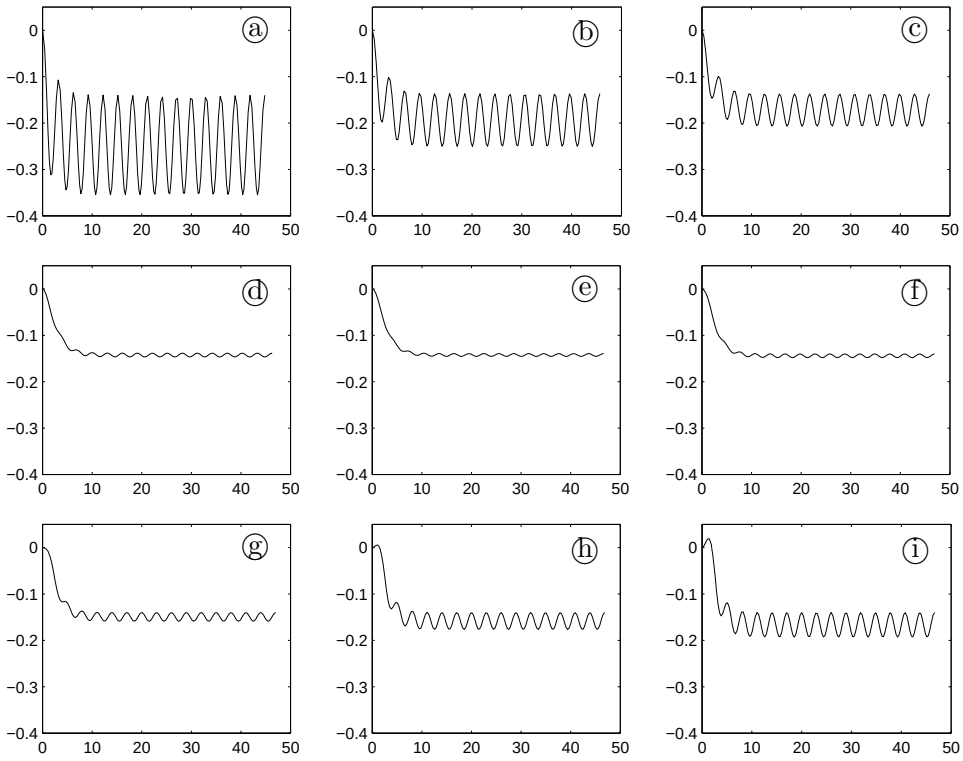

FIG. 8. Typical surface profiles from the right branch. Only half of a wavelength is shown.

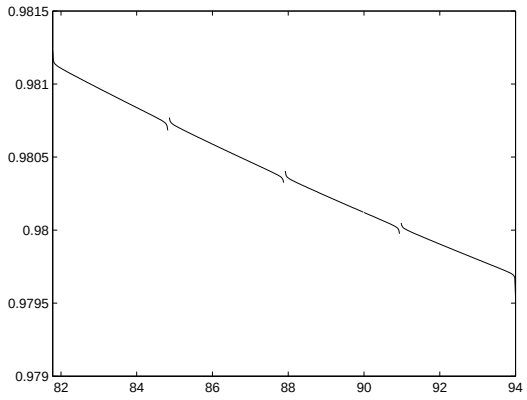

FIG. 9. Value of $1/F^2$ versus the wavelength when $u_0 = 0.97$ and $\beta = 0.07$.

the curvature of the free surface at $\phi_{N-1} = l/2$ as a measure of the amplitude of the ripples in the tail. We denote this parameter by J. Values of J versus β for $l = 99.58$ and $F = 1.03$ are shown in Figure 10. These results and similar ones obtained for other values of l and F strongly suggest that $J \neq 0$ for $\beta \neq 0$ and that there are therefore no true solitary waves (i.e. solitary waves for which the free surface is flat in the far field). A qualitatively similar

result was found in[15] for gravity-capillary waves.

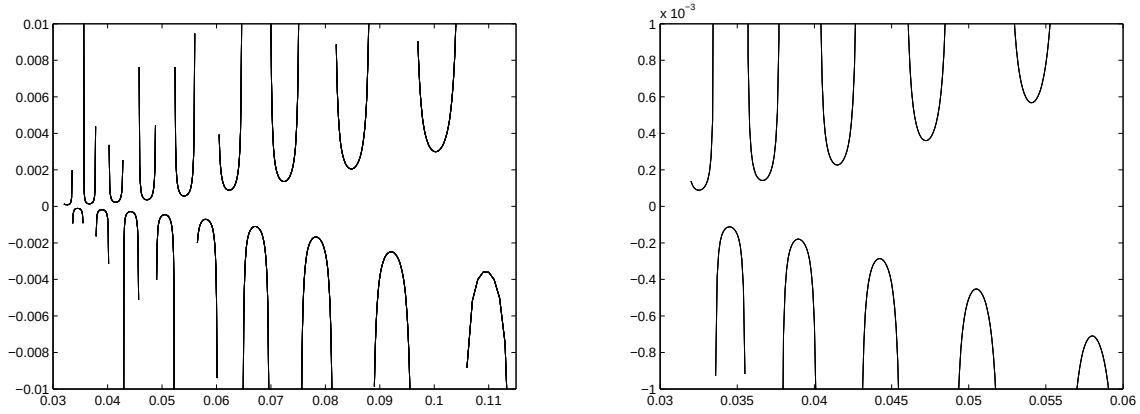

FIG. 10. Value of the parameter J versus β when $l = 99.58$ and $F = 1.03$.

V. COMPARISON WITH THE KIRCHHOFF-LOVE MODEL AND THE PROBLEM OF GRAVITY-CAPILLARY WAVES

A. The Kirchhoff-Love model

We may compare the results from the previous section to the ones produced by the KL model which is defined by (6). We follow the numerical procedure of Section III to simulate the solutions.

In Figure 11 we plot values of $1/F^2$ versus the wavelength l for $A = 0.14$ and $\beta = 0.07$. One can see that there are again two different sub-branches for each family. One slight difference is that the two curves in each family do not intersect in Figure 11 whereas they do in Figure 4. Apart from this, the two graphs are qualitatively similar.

Furthermore, we can also use the KL model and fix the velocity u_0 instead of A. The result is shown in Figure 12. This is qualitatively similar to what we have seen in Figure 9.

B. Gravity-Capillary problem

Generalised solitary waves have been found before in the study of gravity-capillary waves (see[14] and and[16] for a review). We present in this section a comparison of our results for flexural-gravity waves with those of gravity-capillary waves.

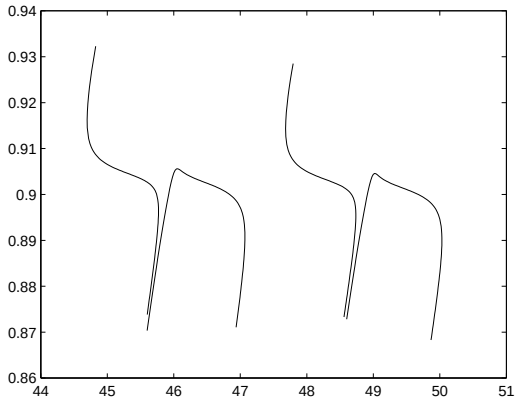

FIG. 11. Value of $1/F^2$ versus the wavelength when $A = 0.14$ and $\beta = 0.07$.

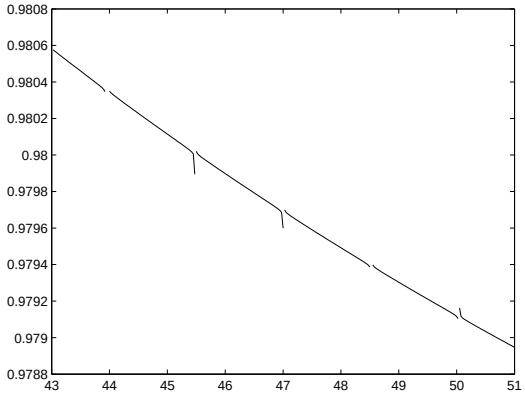

FIG. 12. Value of $1/F^2$ versus the wavelength when $u_0 = 0.97$ and $\beta = 0.07$.

For gravity-capillary waves, (1) is replaced by

$$P = -T\kappa, \tag{39}$$

where T is the surface tension. Using again c as the reference velocity and Q/c as the reference legnth, (17) becomes

$$\frac{1}{2}e^{2\tau} + \frac{1}{F^2}\int_0^{\phi} e^{-\tau(\varphi)}\sin[\theta(\varphi)]d\varphi - \bar{\tau}\kappa = B, \tag{40}$$

where

$$\bar{\tau} = \frac{T}{\rho Q c} \tag{41}$$

is the Bond number.

The remaining equatoins are unchanged and numerical results can be obtained by the procedure of Section III. Values of $1/F^2$ versus l are presented in Figure 13 and Figure 14. The results from Figure 14 agree with those found in[14]. Two sub-branches are again found in Figure 13. These results are qualitatively similar to those obtained in the previous sections for flexural-gravity waves.

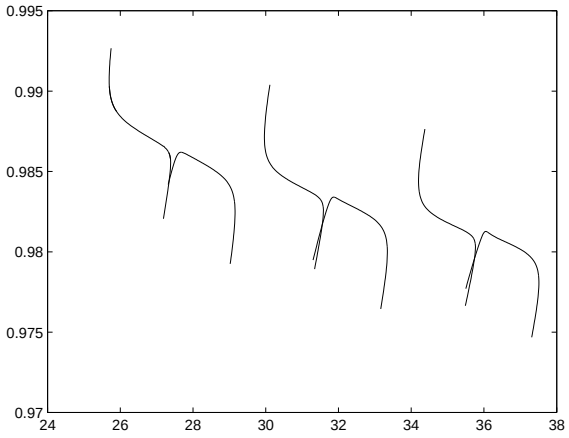

FIG. 13. Value of F versus l when $A = 0.14$ and $\tau = 0.24$.

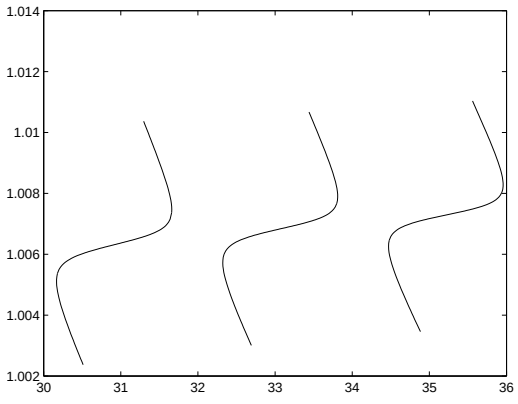

FIG. 14. Value of F versus l when $u_0 = 0.97$ and $\tau = 0.24$.

VI. CONCLUSION

We have presented numerical computations of nonlinear periodic waves and of generalised solitary waves propagating under an elastic sheet. Most of the results were obtained for the Plotnikov-Toland model. We have provided numerical evidence that there are no true solitary waves (i.e. solitary waves with a flat free surface in the far field). Our findings were then compared with those obtained with the simplified KL model and with computations of gravity capillary waves.

ACKNOWLEDGMENTS

The author Tao Gao has been awarded the George Jessel Scholarship given by the Department of Mathematics, University College London.

REFERENCES

[1]A. Korobkin, E. I. Părău, and J.-M. Vanden-Broeck, "The mathematical challenges and modelling of hydroelasticity," Philos. Trans. R. Soc. Lond. A **369**, 2803–2812 (2011).

[2]L. K. Forbes, "Surface waves of large amplitude beneath an elastic sheet. part 1. high-order series solution," Journal of Fluid Mechanics **169**, 409–428 (7 1986), ISSN 1469-7645.

[3]L. K. Forbes, "Surface waves of large amplitude beneath an elastic sheet. part 2. galerkin solution," Journal of Fluid Mechanics **188**, 491–508 (2 1988), ISSN 1469-7645.

[4]E. I. Părău and F. Dias, "Nonlinear effects in the response of a floating ice plate to a moving load," Journal of Fluid Mechanics **460**, 281–305 (2002).

[5]E. I. Părău and J.-M. Vanden-Broeck, "Three-dimensional waves beneath an ice sheet due to a steadily moving pressure," Philos. Trans. R. Soc. Lond. A **369**, 2973–2988 (2011).

[6]P. A. Milewski, J.-M. Vanden-Broeck, and Z. Wang, "Hydroelastic solitary waves in deep water," Journal of Fluid Mechanics **679**, 628–640 (6 2011), ISSN 1469-7645.

[7]P. A. Milewski, J.-M. Vanden-Broeck, and Z. Wang, "Steady dark solitary flexural gravity waves," Philos. Trans. R. Soc. Lond. A **469** (2013).

[8]J.-M. Vanden-Broeck and F. Dias, "Gravity-capillary solitary waves in water of infinite depth and related free-surface flows," Journal of Fluid Mechanics **240**, 549–557 (6 1992), ISSN 1469-7645.

[9]J.-M. Vanden-Broeck and E. I. Părău, "Two-dimensional generalized solitary waves and periodic waves under an ice sheet," Philos. Trans. R. Soc. Lond. A **369**, 2957–2972 (2011).

[10]P. I. Plotnikov and J. F. Toland, "Modelling nonlinear hydroelastic waves," Philos. Trans. R. Soc. Lond. A **369**, 2942–2956 (2011).

[11]P. Guyenne and E. I. Părău, "Computations of fully nonlinear hydroelastic solitary waves on deep water," Journal of Fluid Mechanics **713**, 307–329 (2012).

[12]Z. Wang, J.-M. Vanden-Broeck, and P. A. Milewski, "Two-dimensional flexural–gravity waves of finite amplitude in deep water," IMA Journal of Applied Mathematics(2013).

[13]J. R. Wilton, "On ripples," The London, Edinburgh, and Dublin Philosophical Magazine and Journal of Science **29**, 688–700 (1915).

[14]J. K. Hunter and J.-M. Vanden-Broeck, "Solitary and periodic gravitycapillary waves of finite amplitude," Journal of Fluid Mechanics **134**, 205–219 (1983).

[15]A. R. Champneys, J.-M. Vanden-Broeck, and G. J. Lord, "Do true elevation gravity–capillary solitary waves exist? a numerical investigation," Journal of Fluid Mechanics **454**, 403–417 (2002).

[16]J.-M. Vanden-Broeck, *Gravity-capillary free-surface flows* (Cambridge University Press, 2010).